Median and spatial low-pass filtering in ultrasonic computed tomography

R. M. Schmitt, C. R. Meyer, P. L. Carson, and B. I. Samuels

Department of Radiology, University of Michigan Medical Center, Ann Arbor, Michigan 48109

To reduce noise- and reconstruction-related artifacts in ultrasound computed tomography, the use of combined median and Hamming-weighted spatial low-pass filtering is evaluated. The evaluation of the reconstruction filters uses both computer-generated projections of a known object with the least mean-square error criterion as well as a more subjective evaluation of conventional ultrasonic attenuation and speed of sound images.

I. INTRODUCTION

Imaging of the female breast by means of ultrasonic computed tomography (UCT) is under current investigation for use as a clinical diagnostic tool for breast cancer detection.[1,2]

UCT images are maps of tissue speed of sound and attenuation of sound through coronal planes of the breast. The images reconstructed from time-of-flight (TOF) and attenuation projections suffer from noise- and reconstruction-related artifacts. Reflection, refraction, and diffraction of the interrogating ultrasound beam in complex inhomogeneous objects lead to anomalous variations in estimates of attenuation and speed of sound. Random, Gaussian-distributed noise is introduced in the analog signal processing chain while shotlike impulse noise is generated by mechanical stepping motors. UCT speed of sound imaging is especially susceptible to impulse noise, which results in bright and dark streaks through the image. Reconstruction aliasing artifacts may rise when the attenuation or time-of-flight projections contain abrupt discontinuities, where the spatial sampling rate is insufficient for sampling these sharp edges.

In this paper, we report on the results of the use of a combined median and Hamming spatial low-pass filter for reduction of disturbances intrinsic to UCT.

II. METHODS

A. General

In x-ray CT, it has been shown that the use of Hamming-weighted spatial low-pass filter eliminates aliasing reconstruction artifacts.[3] In addition, low-pass filtering suppresses high-frequency (salt and pepper) noise. It is also known that the nonlinear, median filter of suitable length eliminates impulse noise without substantial loss in high-frequency content and blurring of the image.[4]

Thus by using an appropriate combination of both median- and low-pass filtering, it is possible to suppress artifacts and noise without substantial loss in sharpness.

The evaluation of filters using clinical images alone is difficult because the true imaged object is unknown and because true observer performance studies are time consuming and expensive. For the primary evaluation, we applied the filters on computer-generated projections of a known object and computed the least mean-square error criterion for evaluation. Reconstructions of the known object as well as actu-

al breast scans then were used to confirm the resulting filters as subjectively acceptable for use in patient studies.

UCT images reconstructed using the Ramachandran Lakshminarayan filtered backprojection algorithm (RAM-LAK)[5] are the result of a multistep procedure. First, the projections of the object at different angles are acquired. The projections are filtered by the so-called rho filter in the spatial frequency domain and then backprojected. In all the following examples, the projections are sampled at 8 cm^{-1} corresponding to a Nyquist frequency of 4 cm^{-1}.

B. Median filter

Median filtering can be performed after each step, but we chose to apply it only on projections after acquisition. This restriction will be discussed later. A one-dimensional median filter of window length N ($N =$ odd) replaces the value A_m in a sequence to be filtered by the median of the subsequences $A_{m-(N-1)/2},...,A_m,...,A_{m+(N-1)/2}$. Figure 1 illustrates the effect of median filtering on some arbitrary sequences.

The most useful property of this filter is that it preserves edges while reducing impulse noise. A detailed description of the properties and applications of median filtering is given by Refs. 4 and 6.

C. Hamming filter

As mentioned above, the main reason to introduce a spatial low-pass filter is to suppress Gibb's "ringing" due to aliasing error. It has been shown[3] that the ringing can be
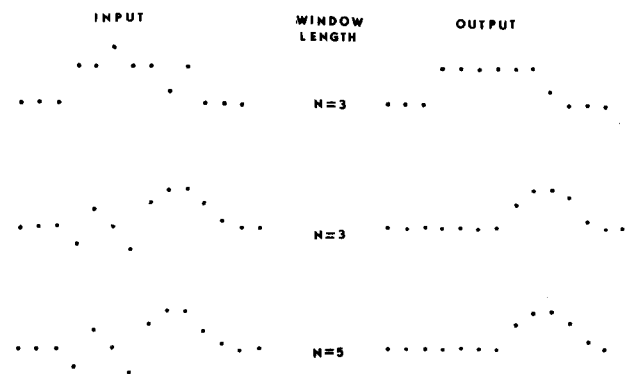

FIG. 1. Effect of median filtering: arbitrary sequences (left) are filtered (right) by median filters of window length $N = 3$ and $N = 5$.

removed by multiplying the rho filter in the frequency domain by a Hanning-weighted window:

$$H(f) = |f|[0.5 + 0.5 \cos(f/f_s)],$$

where f_s is the sampling frequency. In contrast to this, we employ a modified window, the Hamming window. This filter nearly achieves optimal performance in terms of ratio of sidelobe reduction to resolution loss.[7] It is given by

$$(f) = |f|[0.54 + 0.46 \cos(f/f_{co})],$$

where f_{co} is the cutoff frequency at which the filter reaches a minimum value. In the region from the minimum to the Nyquist frequency $f_s/2$, the filter is zero.

D. Computer-generated phantom

To evaluate different filters quantitatively for their efficiency in reduction of image degradation, ideal projections of a simple phantom are calculated. This phantom models the coronal plane of a breast having three circular lesions (fat lobule, cyst, and cancer tissue) surrounded by water. Figure 2 depicts the geometric dimensions of the phantom and the attenuation and velocity coefficients chosen.

Speed of sound and attenuation images of the simulated phantom without noise are shown in Figs. 3(a) and 3(b) we reconstructed with only the rho filter. Gaussian, pseudorandom noise sequences are then added to the original attenuation projections. Two powers of noise were chosen to yield signal-to-noise power ratios (SNR) of 20 (5% noise added) and 3.3 (30% noise added) for a nonattenuated signal. The reconstructed (filtered backprojection) attenuation image at 5% noise is shown in Fig. 3(c). In order to simulate streak artifacts common in our clinical images, one randomly selected ray from each time-of-flight projection is set to the maximum TOF in the projection. This simulates the effect of failing to stop the TOF time interval counter. The reconstructed speed of sound image from these projections is shown in Fig. 3(d).
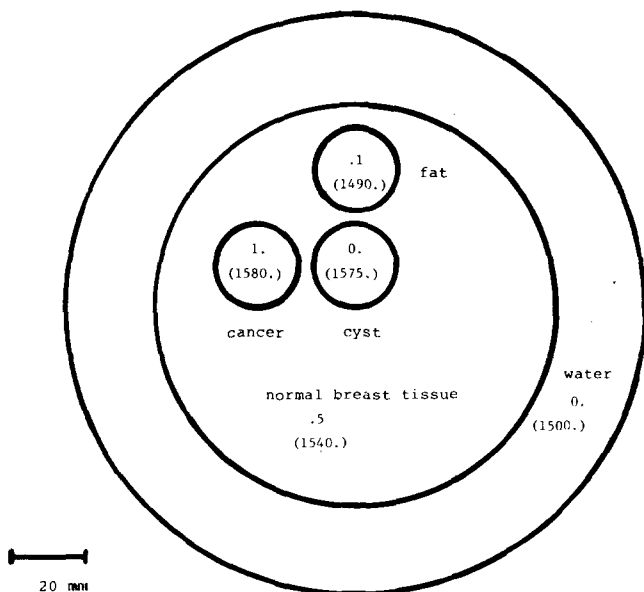

FIG. 2. Shape and numerical values of the computer-generated breast phantom. The ultrasonic attenuation of the three lesions and the normal breast tissue is given in dB/cm/MHz and the speed of sound in m/s.
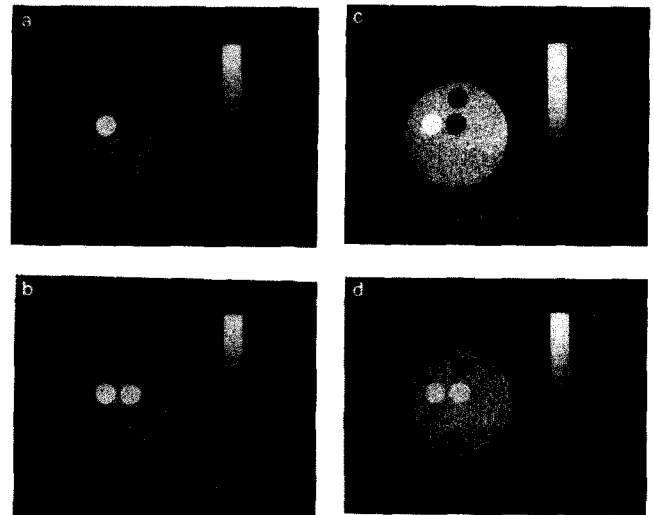
FIG. 3. Reconstructed (filtered backprojection) attenuation (upper row) and speed of sound phantom (lower row) without noise (left), and with noise added (right).

III. RESULTS
A. Projections and images

The effects of median filters of window length $N = 3$ to $N = 7$ on an attenuation projection of the simulated phantom prior to rho filtering is shown in Figs. 4 and 5. The percentage of Gaussian noise added to the noise-free projections [Figs. 4(a) and 5(a)] is 5% in Figs. 4(b)–4(e) and 30% in the Figs. 5(b)–5(e). In Fig. 5 an increasing clustering effect can be observed easily when the window length of the median filter increases.

Figure 6 shows rho-filtered attenuation projections demonstrating the efficiency of the Hamming and median filters in the case of 5% noise. We note that median filtering is performed before the projections are rho filtered. Figure 6(a) represents the original, unfiltered projection. The boost of high spatial frequencies by the rho filter can be seen. Figure 6(b) demonstrates that the periodic high-frequency noise (ringing) is completely removed by weighing the rho filter with a Hamming window. Figure 6(c) depicts the case when random noise (5%) is added. Figures 6(d) and 6(e) show the effect of Hamming filtering (cutoff frequency f_{co} at 3 and 2 cycles/cm, respectively). Figures 6(f)–6(h) show the effect of median filtering. By comparing both series in Fig. 6, it is clearly demonstrated that a Hamming filter is more effective in the suppression of random noise and ringing than the median filter, but it degrades the projection by removing desired high-frequency content.

In order to keep resolution degradation as small as possible, while removing noise, cutoff frequencies between the Nyquist and the sampling frequency were investigated for attenuation reconstructions. Lower cutoff frequencies were investigated with the speed of sound data because objective measurements as well as subjective impressions obtained from our human subject images show that attenuation images contain more information at higher frequencies than the leading edge speed of sound images employed in current clinical trials.
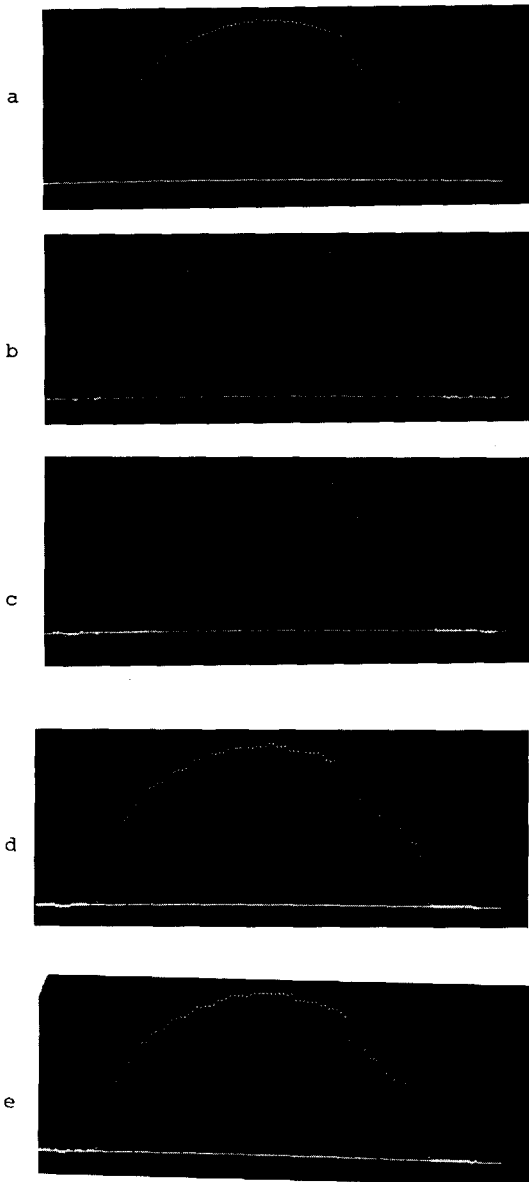
FIG. 4. Effects of median filtering on synthetic projection prior to the rho filter. This series shows the projection without noise (a), with 5% Gaussian, pseudorandom noise added (b), and then median filtered by a window length of $N = 3$ (c), $N = 5$ (d), and $N = 7$ (e).

FIG. 5. Effects of median filtering as in Fig. 4 but with 30% noise added to the projections.

The reduction of attenuation image degradation using Hamming windows with and without median filtering is depicted quantitatively in Fig. 7. The true object from which the projections are calculated is compared to the filtered and reconstructed images using the mean-square error (MSE) as a quantitative measure. We observe that the major reduction of image degradation is achieved when a Hamming window (cutoff frequency $f_{co} = 6$ cm^{-1}) and a three- or five-point median filter is used. Lower cutoff frequencies reduce the MSE only slightly. Clearly this result depends on the frequency content of the object and the amount of noise. When the frequency content in the object decreases, a lower cutoff can be used.

In speed of sound projections, a median filter is ideal for removing impulse noise whereas a Hamming filter with a cutoff at the Nyquist rate (4 cm^{-1} in these examples) is needed for strong suppression of Gibb's phenomenon and random noise. In Fig. 8(a), the noisy attenuation phantom is
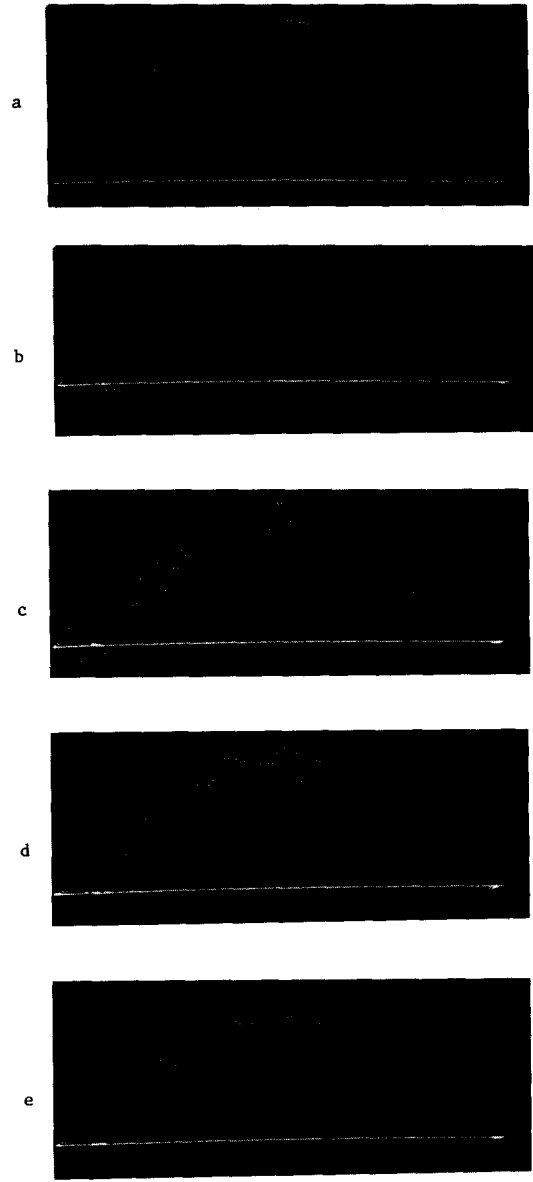
reconstructed using a Hamming window ($f_{co} = 6$ cm^{-1}) and a three-point median filter. The speed of sound phantom is reconstructed in Fig. 8(b) with a Hamming window ($f_{co} = 4$ cm^{-1}) and a three-point median filter, respectively.

B. Clinical images

Two different sets of filter combinations were applied to seven attenuation and seven speed of sound images obtained from four patients. The set applied to attenuation images was obtained by combining an N-point median filter of $N = 1$ (i.e., no filter), $N = 3$, and $N = 5$ with Hamming windows having cutoff frequencies at 8, 6, and 4 cm^{-1} and no spatial filter. A similar set was applied to the speed of sound images, whereby the cutoff frequencies were 4,3, and 2 cm^{-1}.

Figure 9 shows examples of human breast images resulting from median and Hamming filter combinations applied to attenuation [Fig. 9(a)] and speed of sound [Fig. 9(d)] projections. The generally increased filtering from left to right
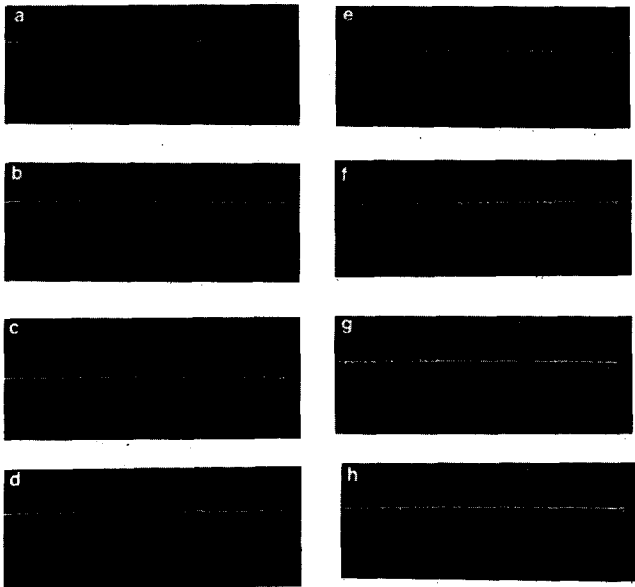
FIG. 6. Effect of median and Hamming filtering after the rho filter is applied. The noiseless projection (a) shows a high-frequency superimposed to the projection due to the aliasing error (ringing artifact). The high frequency is removed when the rho filter is multiplied by a Hamming window having a cutoff frequency of 4 cm^{-1} (b). Also shown is the rho-filtered projection with 5% noise (c), then Hamming filtered with a cutoff of 3 cm^{-1} (d), 2 cm^{-1} (e), or median filtered using a window length of $N = 3$ (f), $N = 5$ (g), and $N = 7$ (h).

FIG. 8.(a) A combination of an $N = 3$ median filter and a Hamming window $(f_{co} = 6$ cm$^{-1})$ is applied to the noisy attenuation projections of Fig. 4(c). (b) An $N = 3$ median filter with Hamming window $(f_{co} = 7$ cm$^{-1})$ is applied to noisy speed of sound projection of Fig. 4(d).

shows the annoying loss of image sharpness in both Figs. 9(e) and 9(f) on the far right. In images 9(b) and 9(d), many of the streak artifacts and other noise at high spatial frequencies have been eliminated without apparently significant loss in sharpness. Contouring, i.e., noticeable regions with constant image gray level, is apparent in the most noise-free speed of sound images 9(e) and 9(f) only because of the limited dynamic range of the four-bit display controller on the research system.
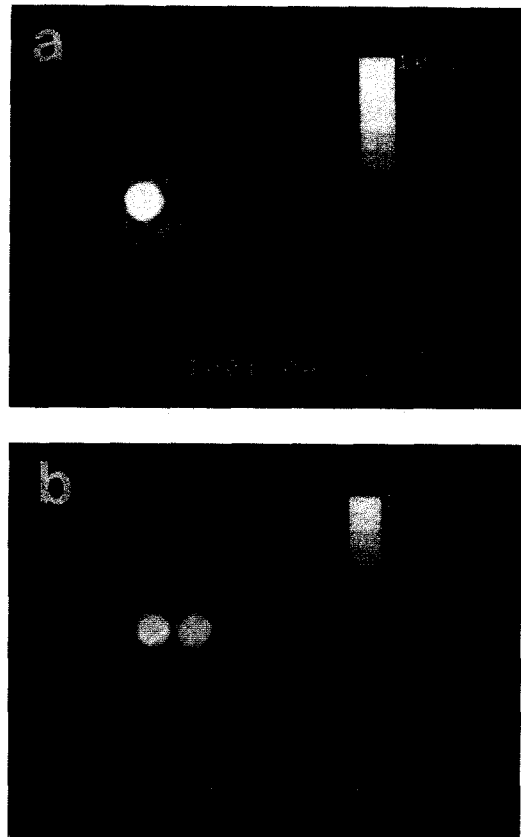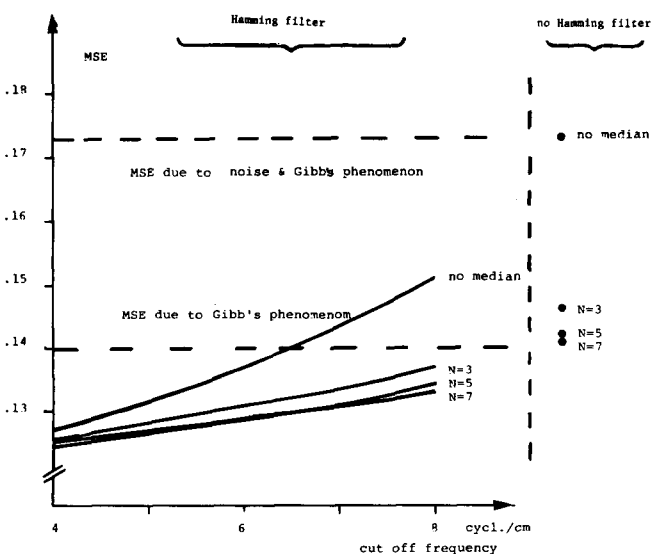

FIG. 7. Effectiveness of Hamming and/or median filtering in reducing image degradation (MSE) due to noise- and reconstruction-related artifacts. MSE image degradation is the mean-square difference between the true and the reconstructed, filtered image.

Two radiologists and two radiological physicists (and one engineer) evaluated the filtered breast images visually. They were asked to compare the filtered to the unfiltered images and to pick a filter combination with the smallest amount of image degradation. An $N = 3$ median filter combined with 8-cm^{-1} cutoff frequency was the preferred filter for attenuation images, while for the somewhat lower resolution speed of sound images an $N = 3$ median filter combined with 3-cm^{-1} cutoff was chosen. There was little variance in the chosen filter across the different images and different observers. However, a wide range of filter combinations were thought to be acceptable by two of the observers, i.e., the number of points in the median filter and/or cutoff frequencies varied by only one step.

IV. CONCLUSIONS

The combination of a median and Hamming-weighted, spatial low-pass filter considerably reduces image degradation due to impulse noise and more continuous distributed noise and reconstruction artifacts. Where the object spatial frequencies detected by the system approach or exceed one-half the spatial sampling frequency, as in our attenuation projections, the number of median filter point and the Hamming or other low-pass filter cutoff frequency should be no higher than is necessary to reduce the worst of the noise. To

(a)   **(b)**   **(c)**
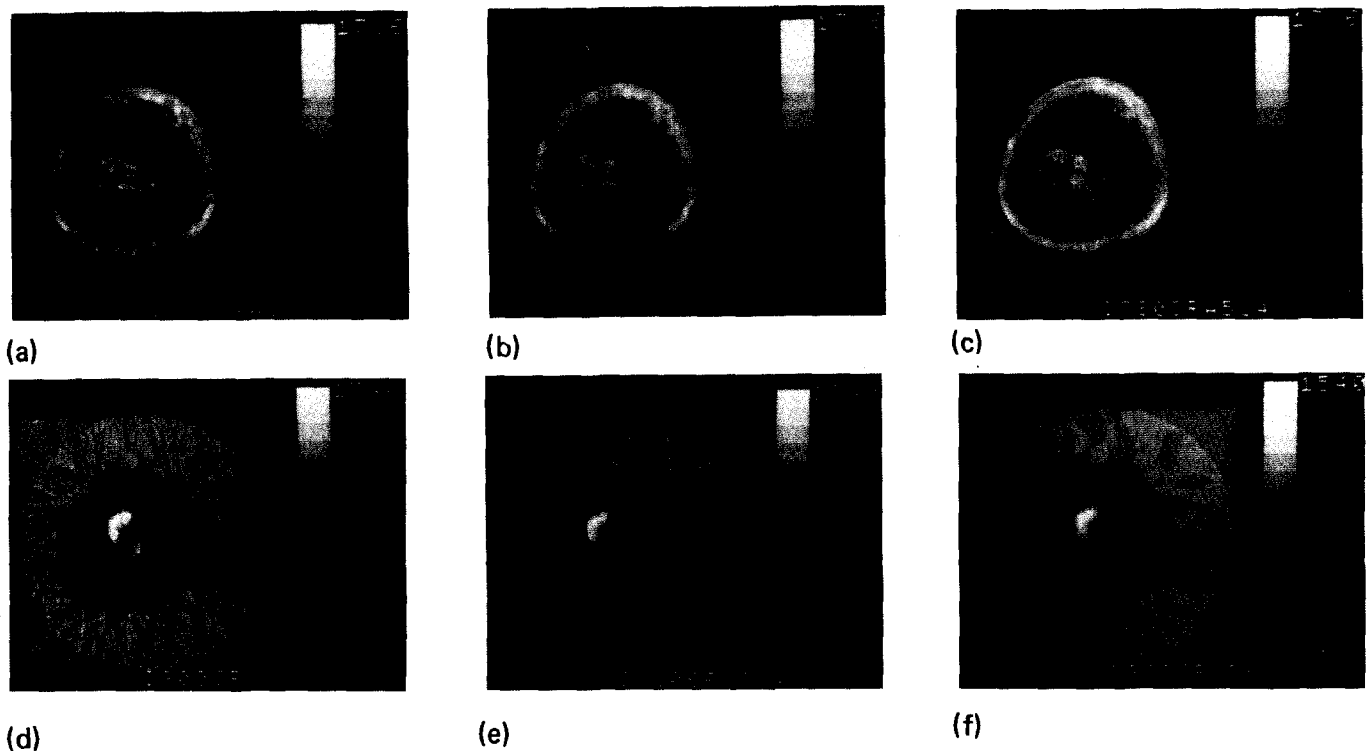
(d)   **(e)**   **(f)**

FIG. 9. Median and Hamming filters applied to nonfiltered images of attenuation (a) and speed of sound (d) of a human breast. The median filter window length N and the Hamming cutoff frequency f_{co} in these combinations are (b) $N = 3, f_{co} = 4$ cm^{-1}; (c) $N = 5, f_{co} = 8$ cm^{-1}; (e) $N = 3, f_{co} = 4$ cm^{-1}; and (f) $N = 5, f_{co} = 2$ cm^{-1}.

accomplish this on our UCT system, the cutoff frequency was chosen at 6 cm^{-1} for attenuation and 3 cm^{-1} for speed of sound, compared with the Nyquist frequency of 4 cm^{-1}. A three-point median filter performed well for both images. The lower cutoff frequency was preferable with the speed of sound images because higher spatial frequencies were not present in the object signal. However, recent experiments with another arrival time measurement technique have provided resolution in speed of sound images at least equal to that of the attenuation images.[8]

There are several conclusions regarding where the filters should be applied in the reconstruction process. For computational efficiency, it seems obvious to combine the Hamming filter with the rho filter, when the filtered backprojection algorithm is used. Since the median filter is nonlinear, the order of its implementation in a sequence of filtering steps is important. We believe there are at least three important reasons median filters should be applied before the projections are rho filtered. First, the noise is reduced before it is amplified by the rho filter. Second, on locations in the object where the attenuation or the velocity is changing the rho filter introduces impulselike structures containing true image content. Such structures would be removed by the median filter, resulting in image degradation. Third, if the median

filter is applied to the final image, an increase of computational time will result, since an N-point median filter requires finding the median value in an N by N grid centered on each point in the image. For M pixels in the image, the number of computer operations would be proportional to $M \times N \times N$. Implementation of the same filter on the projections, rather than the image, requires only the median value of the N points centered on each ray in each projection. Since the total number of rays is approximately equal to the number of image pixels M, the number of computer operations to implement the filter on the projections is proportional to $M \times N$.

[1] P. L. Carson, C. R. Meyer, A. L. Scherzinger, and T. V. Oughton, Science **214**, 1141 (1981).
[2] J. F. Greenleaf and R. C. Bahn, IEEE Trans. Biomed. Eng. **28**, 177 (1981).
[3] D. A. Chessler and S. J. Riederer, Phys. Med. Biol. **20**, 632 (1975).
[4] N. C. Gallagher and G. L. Wise, IEEE Trans. Acoust. Speech Signal Process. **29**, 1136 (1981).
[5] G. N. Ramachandran and A. V. Lakshminarayanan, Proc. Natl. Acad. Sci. U. S. **68**, 2236 (1971).
[6] *Topics in Applied Physics*, edited by T. S. Huang (Springer, Berlin, 1981), Vol. 43.
[7] F. J. Harris, Proc. IEEE **66**, 51 (1978).
[8] T. L. Chenevert, D. I. Bylski, P. L. Carson, C. R. Meyer, P. H. Bland, D. D. Adler, and R. M. Schmitt, Radiology **152**, 155 (1984).